Laser micro-machining of freeform surfaces

Karkantonis, Themistoklis; Penchev, Pavel; Nasrollahi, Vahid; Le, Hoang; See, Tian; Bruneel, David; Ramos-de-Campos, Jose; Dimov, Stefan

DOI:
10.1016/j.precisioneng.2022.08.009

Document Version
Peer reviewed version

Citation for published version (Harvard):
Karkantonis, T, Penchev, P, Nasrollahi, V, Le, H, See, T, Bruneel, D, Ramos-de-Campos, J & Dimov, S 2022, 'Laser micro-machining of freeform surfaces: accuracy, repeatability and reproducibility achievable with multi-axis processing strategies', *Precision Engineering*, vol. 78, pp. 233-247.
https://doi.org/10.1016/j.precisioneng.2022.08.009

Laser micro-machining of freeform surfaces: accuracy, repeatability and reproducibility achievable with multi-axis processing strategies

Themistoklis Karkantonis[1, *], Pavel Penchev[1], Vahid Nasrollahi[1], Hoang Le[1], Tian Long See[2], David Bruneel[3], Jose A. Ramos-de-Campos[3], Stefan Dimov[1]

[1] *Department of Mechanical Engineering, School of Engineering, The University of Birmingham, Birmingham, B15 2TT, UK*

[2] *The Manufacturing Technology Centre Ltd, Coventry, CV7 9JU, UK*

[3] *LASEA S.A., Liège Science Park, Rue Louis Plescia 31, 4102 Seraing, Belgium*

[*] Corresponding author at: Department of Mechanical Engineering, School of Engineering, The University of Birmingham, Birmingham, B15 2TT, UK.

E-mail address: TXK880@bham.ac.uk (T. Karkantonis)

Abstract

The requirements that complex 3D miniaturised components have to satisfy are constantly increasing for various application areas, e.g. in aerospace, biomedical and electronics, and hence there is a sustained drive to broaden the capabilities of precision manufacturing processes. In this regard, state-of-the-art Laser Micro-Machining (LMM) systems have been attracting significant industrial interest with their emerging capabilities for multi-axis machining. However, intrinsic limitations of component technologies of such systems can impact the machining accuracy, repeatability, and reproducibility (ARR), especially in complex processing strategies requiring the simultaneous use of multiple axes, and consequently to affect the overall processing uncertainty. Herein, the aim of this research is to propose a systematic method for assessing the overall performance of such LMM systems when they are deployed for laser structuring/patterning/texturing of freeform surfaces. In particular, the method employs a series of laser processing tests on spherical samples to quantify the contributions of different error sources on the machining ARR when implementing simultaneous multi-axis processing strategies under quasi-static and dynamic conditions. An experimental validation of the proposed method is conducted on a representative state-of-the-art LMM system and then conclusions are drawn about its capabilities to determine the processing ARR of multi-axis LMM systems. This research provides an insight into the limitations and manufacturing challenges in deploying such systems for the fabrication of complex 3D components.

Keywords: Machining test, Laser micro-machining system, Performance evaluation, Precision metrology, Freeform surface, Multi-axis simultaneous laser processing, Accuracy, Repeatability, Reproducibility, Uncertainty.

1. Introduction

Over the last decade, technological advances in different industrial sectors, i.e. biomedical, aerospace, electronics and telecommunications, have driven the demand for producing highly accurate miniaturised components with intricate geometries [1, 2]. To address these challenging requirements, various conventional and non-conventional manufacturing technologies have been deployed to fabricate high-precision micro-structures/features in products [3-5]. Traditionally, such features were manufactured through CNC micro-milling, however inherent limitations of this technology with respect to tool wear, spindle speed and available cutting tool sizes constrain its broader use.

On the other hand, non-contact chip-less machining processes have attracted the interest of industry and research due to their intrinsic characteristics. Among them, Laser-based Micro-Machining (LMM) can offer an attractive alternative in performing different high resolution operations, e.g. structuring/texturing/scribing, drilling, polishing and cutting, on freeform surfaces in a fully integrated manufacturing platform. Compared to lithographic processes, this technology offers relative higher processing efficiency, flexibility and reliability while it does not require a clean-room environment for its use [6]. At the same time, it is a process that can be used to machine almost any engineering material, such as glass [7], metals [8], ceramics [9] and polymers [10], by selecting a suitable laser source.

Recently, the LMM technology has been extensively deployed as a surface modification technique to fabricate micro/nano structures on planar surfaces of new or existing products and thus to "imprint" attractive surface functionalities, e.g. anti-biofouling [11], anti-corrosion [12], anti-bacterial [13], anti-icing [14], anti-reflective [15], anti-adhesive [16] and cell-adhesion [17]. Despite that, it is recognised that laser machining of micro/nanoscale structures onto complex 3D surfaces with significant variations in their curvature, e.g. on medical implants and contact lenses, is of great importance and could broaden the LMM industrial applications [18-21]. Therefore, multi-axis LMM systems, which combine the capabilities of 5 axes CNC systems together with that of scanning heads, can be used to execute complex 3D laser processing strategies that were considered not achievable until recently.

To date, the most well-recognised approach to texture/structure large freeform/curved surfaces is to apply a tessellation/partitioning method to divide them into planar scanning fields and

layers by taking into account the constraints introduced by the beam delivery sub-systems [22, 23]. In these cases, mechanical stages are used only to position the centre of each field to be normal to the laser beam, and then the scanning head executes the necessary processing strategy. Nonetheless, there are specific challenges/limitations that should be taken into consideration when laser processing 3D surfaces. More specifically, the variations of Beam Incidence Angle (BIA) and Focal Offset Distance (FOD) due to the surface curvature might impact the dimensional accuracy and/or functional characteristics of structures/textures. Therefore, some processing constraints should initially be determined for both factors according to the application-specific requirements and then used to drive the surface partitioning process [24-26]. At the same time, the overall machining accuracy also depends on the component technologies of LMM systems, i.e. mainly determined by the employed optical and mechanical axes, when executing multi-axis processing strategies. Therefore, their machining performance has been evaluated separately or in combination under a "positioning mode" for precision LMM using optical metrology systems [27-29].

Lately, state-of-the-art multi-axis LMM platforms have been introduced to the market that can operate in a "simultaneous mode" and hence enable the synchronous motion control of multiple optical and mechanical axes during the laser processing operations. As a result, this technology enables LMM improvements related to the overall processing uniformity and efficiency, especially when curved or even freeform surfaces are processed. In particular, such operations can benefit and employ the highly accurate mechanical axes and the fast scanning capabilities of optical ones, simultaneously. However, multi-axis simultaneous processing strategies are associated with inferior overall machining accuracy due to the spatial accumulated errors of multiple axes and their interactive effects on tool/beam positioning in regard to the workpiece [30]. An analytical description of the error sources affecting the LMM operations is further elaborated by other researchers [31]. Even though information about Accuracy, Repeatability and Reproducibility (ARR) of optical and mechanical axes are provided in the technical specifications by the manufacturers, it is not possible to estimate the machining ARR when executing multi-axis motions and the uncertainty associated with such processing strategies. Therefore, the use of systematic evaluation procedures for assessing the machines' overall ARR are essential as they are required to determine the geometrical and dimensional tolerances achievable when processing complex 3D components.

In this respect, various test pieces, such as a semi-sphere, a cone frustum in NAS 979 or a S-shaped piece in ISO 10791-7, requiring multi-axis simultaneous machining have been proposed as indirect assessment methods for evaluating the overall performance of conventional 5-axis machine tools under quasi-static and/or dynamic states [32-35]. In such machining tests, the motion errors of all employed axes are combined/superimposed onto the finished part and hence they can be used as a final acceptance test for machine tools after their installation on-site. Nevertheless, a similar verification test has not been reported for LMM systems, yet, most likely because simultaneous multi-axis LMM capabilities have only been introduced to the market, recently. Thus, further efforts are necessary to develop a systematic method for assessing ARR of LMM systems when executing simultaneous multi-axis processing strategies that combine both optical and mechanical axes.

This research reports an investigation into the capabilities of state-of-the-art multi-axis LMM systems that are specially designed and implemented for processing complex 3D components. Firstly, the generic concept for laser texturing/structuring/scribing of freeform/curved surfaces is introduced that offers a higher processing efficiency due to the simultaneous control of both optical and mechanical axes. Thereafter, a generic method is proposed for assessing the impact of different error sources on the ARR of such laser processing setups. An experimental study was conducted to quantify and compare ARR when both optical and mechanical axes were simultaneously utilised in different combinations/processing strategies for precision laser texturing/structuring/scribing operations under quasi-static and dynamic conditions. Lastly, the validity of the proposed method is discussed, and conclusions are made about its capability to assess the performance of multi-axis LMM systems.

2. Multi-axis simultaneous laser processing

In general, there are various types of multi-axis LMM system configurations available on the market, however the most common one includes three linear-axis drivers (X, Y, Z), two rotary-axis drivers (C, B or A) and a galvo scan head. An example of such multi-axis LMM system is provided in Section 4. The basic principles of simultaneous multi-axis LMM are very similar to those in conventional machining. The axes' motions are coordinated, e.g. the movements from an initial to a final position can be defined as machining/beam vectors according to the number of axes involved. For LMM of freeform/curved surfaces, the axes are programmed to start/end their movements at the same time. Compared to conventional machining, the LMM technology involves two additional optical axes (Gx, Gy) realised with beam deflectors

integrated into the galvo scanners. As such, laser texturing/structuring/scribing operations allow variations of FOD and BIA along the beam paths to benefit from their high beam deflection speed. Thus, this inherent characteristic can contribute not only to minimise the overall machining time, but also to circumvent the use of an optical Z module for dynamically refocusing the laser beam on the surface. Nevertheless, the FOD and BIA, i.e. the angle (θ) between the laser beam and the surface tangent at the incident point, variations should be constrained within an effective processing area where their negative side effects do not jeopardise the desired machining performance. As can be seen in Fig. 1a, this area should be equal to or smaller than the lenses' Field of View (FOV) on curved surfaces and is typically defined by the Rayleigh length.

Furthermore, the generation of beam paths with a certain directionality, e.g. vertical, horizontal or diagonal, and the synchronous control of optical and mechanical axes motions has specific requirements and cannot be implemented using stand-alone universal Computer-Aided Design (CAD)/Computer-Aided Manufacturing (CAM) tools. Therefore, specially developed postprocessors are necessary and they should be integrated into existing CAD/CAM packages. They output the programmed movements into beam vectors while considering the points where the laser source should be turned on/off. For clarity, a graphical representation of a geometry projected on a sphere's periphery that should be processed/scribed using simultaneous multi-axis LMM strategy is shown in Fig. 1b. In such processing strategies, the orientation of beam paths and the motion of mechanical axes should be perpendicular to each other. In particular, both optical axes should be deployed to execute the desired processing strategy, whilst the mechanical axes are simultaneously used to maintain the centre of each beam path at the focal plane and the BIA normal to the surface. For processing large surface areas, i.e. when their size along the beam scanning direction exceeds either the laser's effective processing area or lens's FOV, they must be partitioned into multiple scanning fields. In contrast, it should be noted that there is no need for partitioning the surfaces along the mechanical axes trajectory and thus the stitching errors can be reduced when executing multi-axis simultaneous LMM strategies. After partitioning the surfaces, each scanning field is processed individually and then the mechanical stages are deployed to reposition the laser beam between them. Generally, the surface partitioning process can be implemented using algorithms/tools available in most commercial CAD packages by specifying some geometrical constraints [24].

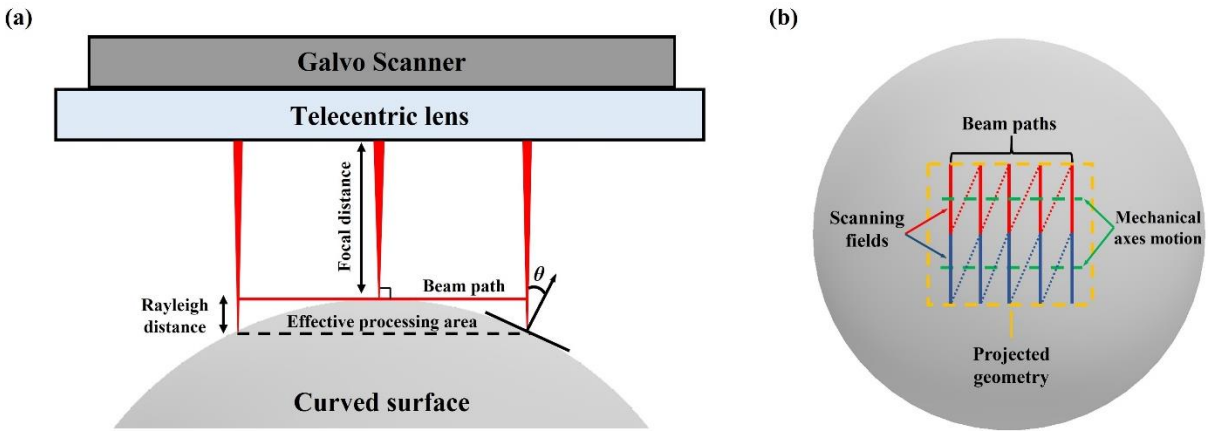

Fig. 1. A schematic representation of: (a) a single beam path on a curved surface; (b) a geometry projected on a spherical surface that should be scribed using a simultaneous multi-axis LMM strategy.

Note: The red and blue dashed lines in (b) represent the motions of optical axes when the laser source is inactive.

3. Methodology

A generic empirical method is proposed for assessing the overall performance of multi-axis simultaneous laser structuring/texturing/engraving operations under both quasi-static and dynamic conditions. An overview of all the steps involved is given in Fig. 2. The prerequisites for implementing this method are to: i) predefine an effective processing window for machining freeform/curved surfaces; and ii) compensate the negative dynamic effects of the optical beam deflectors before investigating the dynamic capabilities of such laser processing setups. These two aspects in the proposed methodology are introduced/discussed briefly in the next two sub-sections for completeness before the generic method for assessing the capabilities of multi-axis LMM systems is described.

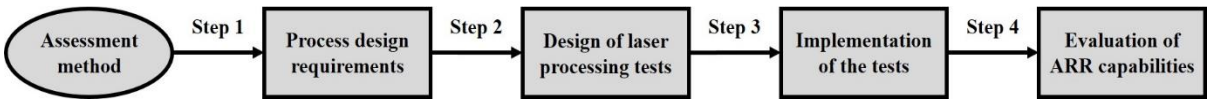

Fig. 2. The sequence of steps to execute the proposed assessment method.

3.1 Effective processing window

In laser processing of freeform/curved surfaces, the beam paths cannot anymore lay fully onto the focal plane (see Fig. 1a) and thus an acceptable range of FOD variations should be defined for obtaining satisfactory machining results. Theoretically, this FOD limit should be equivalent to the Rayleigh length as the laser beam is considered in focus within this range. However, in

the case of LMM operations requiring high precision, any displacements from the focal plane may influence the width and depth of machined structures depending on the used laser source and workpiece material. Therefore, alternative strategies should be followed as proposed in [36] to define the effective processing area by conducting some preliminary laser trials. In brief, these strategies require to scribe a set of structures onto a planar workpiece with varying FODs while BIA is kept normal to the surface. In this way, the impact of FOD on the ablation depth can be quantified and the processing performance satisfactory cut-off value can be determined. An example of such preliminary trials is provided in Sub-section 4.2.

3.2 Dynamic effects of optical beam deflectors

In LMM operations, the optical beam deflectors, i.e. optical axes, are used for steering the laser beam across the workpiece surface and thus they accelerate/decelerate whenever its velocity or motion trajectory has to change. Without applying any compensations, this can have a significant impact on the achievable quality and dimensional accuracy of machined structures. For instance, the existence of acceleration/deceleration regions at the beginning and end of each beam path can result in discrepancies between the desired and actual machined patterns on surfaces as shown in Fig. 3a. At the same time, it can lead to variations in the ablation depth of the machined structures. As can be seen in Fig. 3b, a higher removal rate can be detected in the processed areas where the effects of accelerations/decelerations are present. In reality, such errors are more pronounced at high scanning speeds and are mainly attributed to the inertia of deflectors' driving motors [37]. Therefore, it is essential to counteract the aforesaid negative dynamic effects of beam deflectors prior to investigating the LMM system's ARR capabilities under dynamic conditions. Especially, an empirical method should be used to compensate these dynamic effects and thus to attain a constant velocity along the beam vectors when the laser source is triggered. Firstly, the process requires the acceleration/deceleration regions of the beam deflectors to be determined experimentally using a strategy similar to that proposed in [38]. As such regions are dependent on the set scanning speeds and the specific LMM setups, an example of how they could be determined is provided in Sub-section 4.2. Thereafter, the beam vectors should be adjusted to include these compensations. As a result, accelerations/decelerations occur only in these regions while the laser source is switched off.

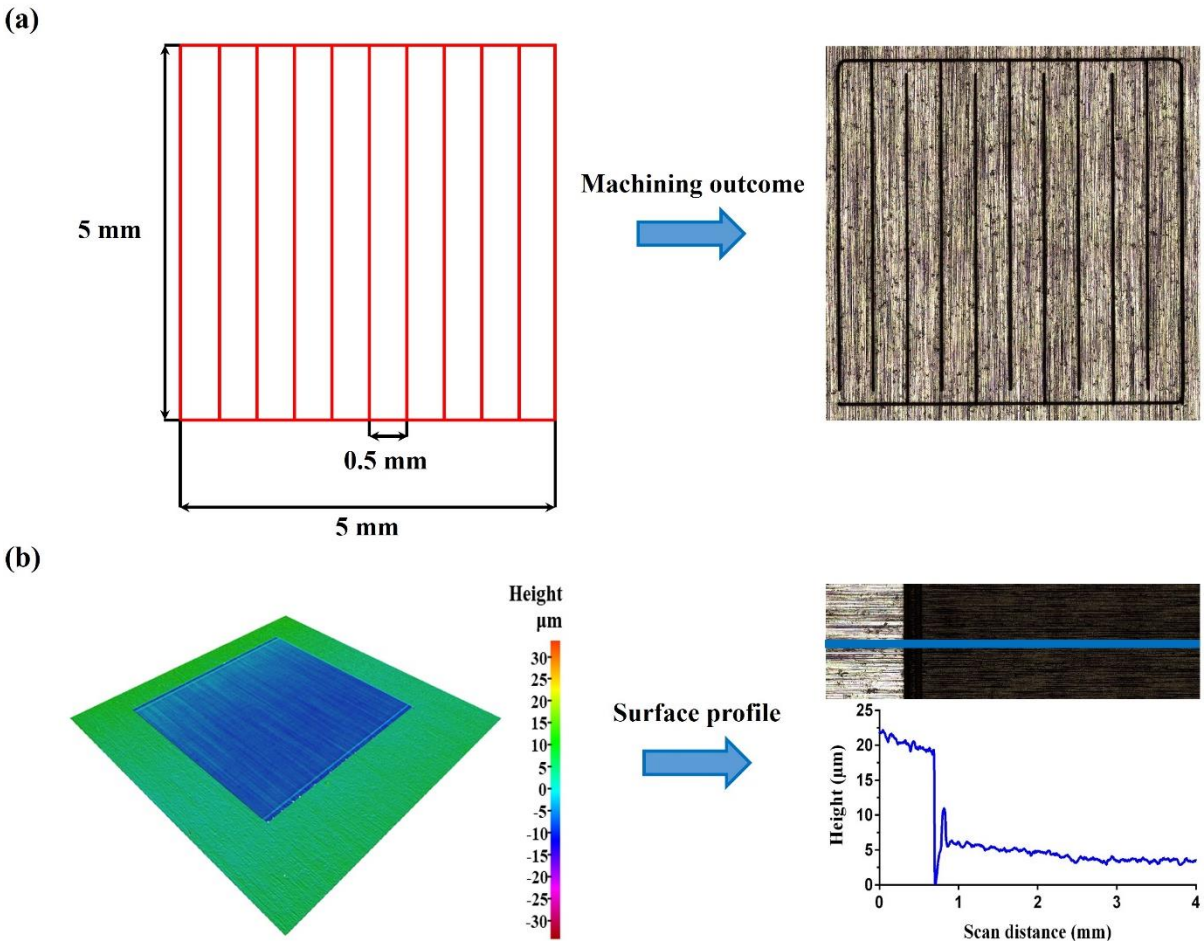

Fig. 3. Negative dynamic effects of beam deflectors at a scanning speed of 500 mm/s without applying any compensation method: (a) dimensional discrepancies between the programmed (red lines on the left side) and the actual beam scribing (line-like structures on the right side); (b) a height map of the processed area (left) and surface profile (right) of a pocket with non-uniform ablation at the walls (beam trajectories change points).

Note: The blue profile in (b) shows the effect of the beam acceleration and deceleration in executing the processing strategies.

3.3 Method for assessing simultaneous multi-axis laser processing strategies

The assessment method is proposed in this research that requires four Laser Processing Tests (LPTs), namely LPT 1, LPT 2, LPT 3 and LPT 4, to be performed onto spherical test pieces to judge the ARR capabilities of LMM systems when conducting simultaneous multi-axis texturing/scribing/structuring operations on curved/freeform surfaces. In particular, this method requires, first, an accurate 3D model of the spherical samples to be created using a CAD/CAM software. Thereafter, a set of four patterns, which should be scribed on the surface in the four LPTs, has to be designed and projected onto it as shown in Fig. 4a. For clarity, each

projected pattern in the set is used for a different test. It is worth noting that the patterns' dimensions should be selected in such a way that they should be within the effective processing area of the laser. In addition, the intrinsic constraints introduced by the rotational ranges of A or B axes should be taken into consideration when selecting their dimensions, too.

The LPTs were specially designed to investigate all available options in executing multi-axis laser texturing/scribing/structuring operations that require simultaneous control of both mechanical and optical axes. Therefore, a different processing strategy should be utilised to process the pattern for each test. For instance, the most common scanning strategies, i.e. vertical, horizontal and diagonal at 45° and - 45° to the horizontal one, which at the same time include all the possible simultaneous combinations of optical and mechanical axes, are depicted in Fig. 4b. For LMM system configurations that include either B or A rotary-axis, the combinations of simultaneous multi-axis motions required to execute the processing strategies in each LPT are summarised in Table 1. Even though this research refers mainly to the most common LMM configuration and scanning strategies, the fundamental idea behind the design of this assessment tests and method can easily be extended to evaluate any type of multi-axis LMM configuration and scanning strategy.

Table 1. The processing strategies with their respective simultaneous axes motions employed in executing the four tests on a LMM system with either B or A rotary-axis.

LPT no.	Scanning strategy	Multi-axis LMM system configurations with	
		B rotary-axis	A rotary-axis
LPT 1	Vertical	C, Gx, Gy	C, Gx, Gy
LPT 2	Horizontal	X, Z, B, Gx, Gy	Y, Z, A, Gx, Gy
LPT 3	Diagonal (45°)	X, Z, B, C, Gx, Gy	Y, Z, A, C, Gx, Gy
LPT 4	Diagonal (- 45°)	X, Z, B, C, Gx, Gy	Y, Z, A, C, Gx, Gy

In all test strategies, a constant offset distance (h_1) between any two consecutive beam scribing vectors should be set to produce line-like structures on the surface with only a single pass. Ideally, this distance should be selected according to the application-specific requirements. However, it should be sufficiently big so that the scribing lines do not overlap even in the case when the maximum predetermined FOD and BIA limits are present. Meanwhile, another set of equally distant (h_2) beam scribing vectors, i.e. three perpendicular to the other ones (see the blue lines in Fig. 4b), should also be added to the tests and then used as reference to evaluate the geometrical accuracy of the scribing lines produced with the former set of beam vectors. Thus, it should be noted that the execution of these beam vectors and the relative positioning

movements between them must be performed only with X and Y mechanical axes due to their higher ARR compared to the optical axes.

Furthermore, the proposed test method aims to assess the ARR capabilities of LMM systems. Therefore, pseudo-repeatability and reproducibility tests should be carried out by repeating the four LPTs on the same and on another spherical sample using the same laser processing parameters, respectively. As such, three sets of identical scribing patterns should be produced on the two samples, namely Pattern Set 1 (PS 1) on sample 1, Pattern Set 2 (PS 2) on sample 1 and Pattern Set 3 (PS 3) on sample 2. Thereby, the ARR capabilities of a LMM system to execute the LPTs should be assessed based on the results obtained from these three Pattern Sets. To judge the overall performance of LMM systems under quasi-static, i.e. with no dynamic influences and servo control limitations, and dynamic states, the whole experimental procedure needs to be conducted at both low (e.g. less or equal to 10 mm/s) and high (e.g. equal or above 100 mm/s) scanning speeds. However, when investigating their dynamic capabilities, the beam vectors should be adjusted as described in the previous sub-section to avoid/minimise the negative dynamic effects associated with optical axes. At the same time, it is necessary to ensure that the compensation for the first beam vector is sufficient to allow a constant velocity to be reached along the mechanical axes at the beginning of each laser processing operation.

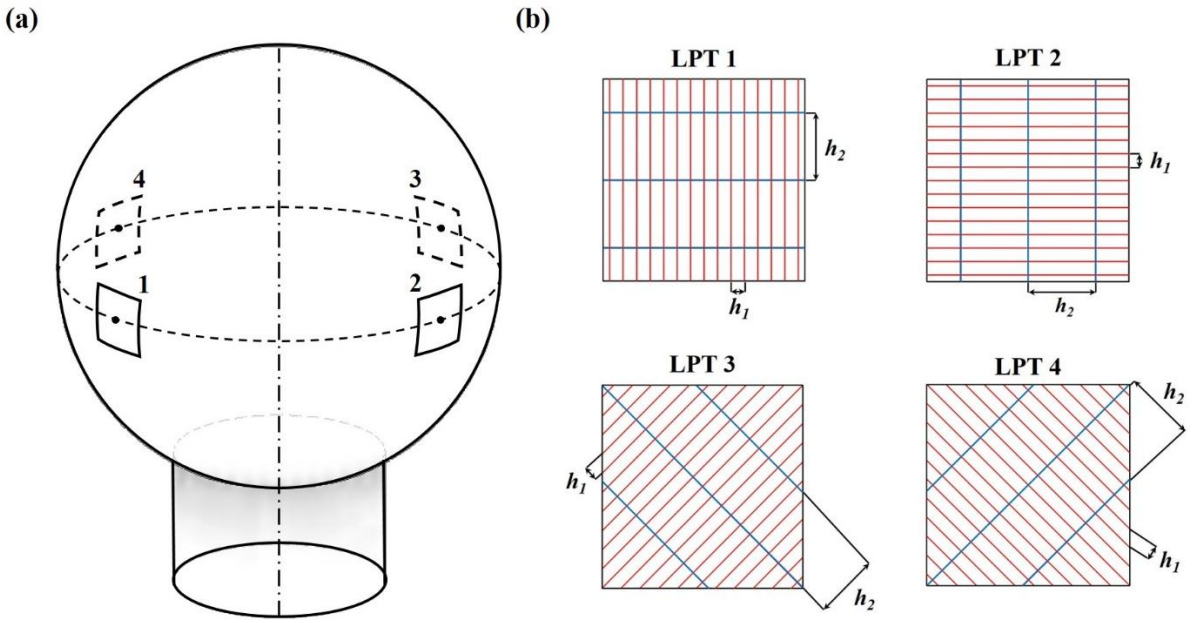

Fig. 4. The LPTs in the proposed method for assessing the performance of different simultaneous multi-axis LMM strategies: (a) a schematic illustration of the patterns that should be scribed on the spherical surface in the four LPTs; (b) the scribing strategies employed to produce the four patterns in the tests.

Due to the contactless nature of the LMM technology, laser texturing/scribing/structuring operations can tolerate some deviations in BIA from normal together with some FOD variations until evident alterations of the machined structures can be observed [39]. As a result, the actual processing errors, i.e. in the width and depth of the scribing lines, may not be truly reflected onto the surface and hence they cannot be quantified accurately. Therefore, only the deviations in the length (d_1), pitch (d_2) and geometrical accuracy of the scribing lines produced with a single pass should be considered in assessing the ARR achievable with the investigated simultaneous multi-axis LMM strategies. However, the d_2 and geometrical accuracy can vary along the scribing lines due to the simultaneous movements of mechanical and optical axes required to execute the programmed beam vectors in the four LPTs. Therefore, their average values should be determined based on multiple measurements taken at different places along the scribing lines. An example on how to measure the three aforementioned parameters is given in Sub-section 4.5. At this point, it should be stated that their geometrical accuracy can be quantified by measuring their perpendicularity (g) against the reference ones produced using only the mechanical stages. Regarding the scribing lines' d_1 and d_2, the processing accuracy should be assessed based on their maximum deviations from their nominal/programmed values. On the other hand, the repeatability and reproducibility should be evaluated by comparing the measured values with their respective average values obtained from samples 1 and 2, respectively. Lastly, to ensure that the ARR capabilities of LMM systems can be quantified in a reliable and repeatable manner using the proposed test method, the uncertainty associated with the employed measuring equipment and procedures must be kept to a minimum. A flowchart is provided in Fig. 5 that summarises the main steps and methodology proposed in this research to evaluate the overall performance of LMM systems.

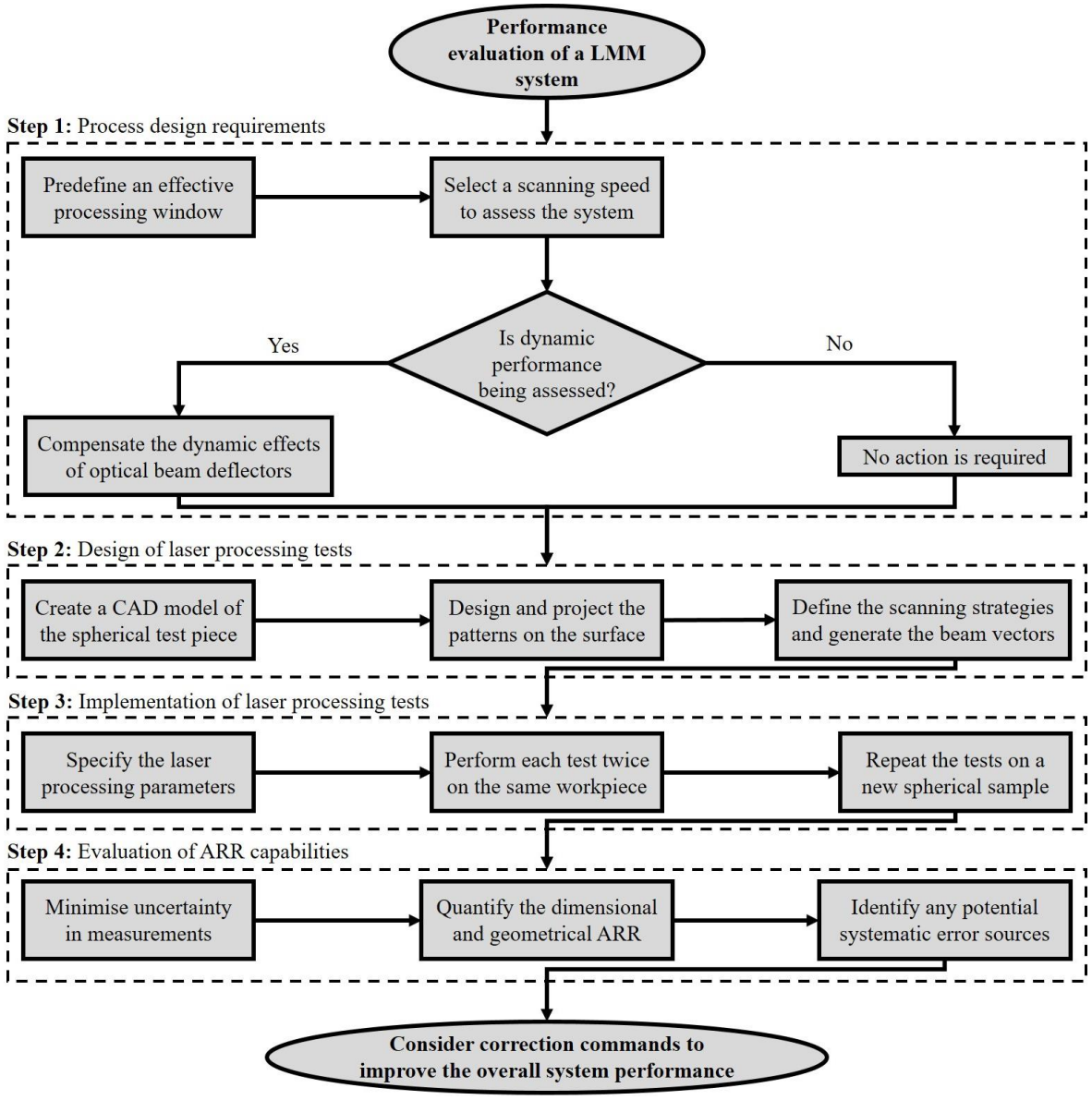

Fig. 5. Flowchart summarising the procedure to evaluate the performance of a LMM system.

4. Pilot implementation

A pilot implementation of the proposed methodology is provided in this section. To demonstrate the applicability of the proposed method, a multi-axis LMM system was selected that was capable of executing the considered LPTs and thus to show what quantitative data about the ARR capabilities of such systems can be obtained.

4.1 Experimental set-up and analysis tools

The experimental trials were conducted on the state-of-the-art LASEA LS4 LMM workstation and its main component technologies, i.e. beam delivery sub-system and the multi-axis setup, are depicted in Fig. 6. In particular, the system is equipped with a high precision stack of two

rotary-axis drivers (B, C) and three linear (X, Y, Z) mechanical stages to tilt, rotate and position the workpiece inside the machine's working envelop. The C rotary stage is on top of the B one and it can rotate continuously, whereas the latter is limited to the range of - 100° to + 30°. In addition, a reconfigurable work-holding device is mounted on the C rotary stage to precisely load and unload the samples. A galvo scan head, mounted on the Z stage, with two optical beam deflectors (Gx, Gy) is incorporated in the beam delivery sub-system that allows the laser beam to be steered with a maximum scanning speed of 50 rad/s. For multi-axis processing strategies, the motions of optical and mechanical axes are fully synchronised and are controlled by a PC-based multi-axis motion controller (Aerotech A3200). To ensure that the beam deflectors operated within their technical specifications, as stated in Table 2, an automated calibration process was carried out prior to the LMM operations. At the same time, the positioning ARR of the linear stages (see Table 2) were measured using a laser interferometer and were then error mapped by the manufacturer during the installation.

Table 2. Technical specifications of component technologies (as provided by the manufacturer) integrated into the LS4 workstation.

Specifications	X/Y axis	Z axis	B axis	C axis	Optical axes
Travel range	500/300 mm	200 mm	-100° to +30°	continuous	640 mrad
Resolution	0.1 μm	1 μm	0.01°	0.01°	10 μrad
Max travel speed	200 mm/s	150 mm/s	200 deg/s	200 deg/s	50 rad/s
Acceleration rate	3000 mm/s^2	1250 mm/s^2	500 deg/s^2	500 deg/s^2	-
Accuracy	± 1 μm	± 1.75 μm	5 arc sec	6 arc sec	± 5 μm
Repeatability	± 0.4 μm	± 1 μm	3 arc sec	3 arc sec	± 10 μrad
Thermal drift	-	-	-	-	± 20 μrad
Tracking error	-	-	-	-	160 μs

Furthermore, the LS4 workstation integrates a 10 W ultrafast femtosecond laser source (Yuja, Amplitude Systems) with a central wavelength of 1030 nm delivering pulse energies up to 100 μJ at 100 kHz, pulse durations in the range from 300 fs to 10 ps, and maximum repetition rates up to 2 MHz. Also, the workstation integrates a 50 W pulsed nanosecond fibre laser (GLPN series, IPG) that operates at a central wavelength of 515 nm. In this research, the experimental work was conducted using the ultrashort pulse laser in order to attain a higher structuring quality, i.e. edge definition, and thus to minimise the measurement uncertainty in quantifying the system's ARR capabilities. Nevertheless, it should be noted that the proposed assessment method can be implemented onto any multi-axis LMM system irrespectively of the laser source integrated into it.

Commercially available aluminium spheres, with a nominal diameter of 40 mm and deviations from sphericity within ± 0.5 μm, were used in this pilot implementation of the proposed method. The spheres were attached to a shaft extension of 15 mm, and they were utilised to evaluate the machining ARR capabilities of the LMM system. The substrates were processed with a nearly Gaussian beam ($M^2 < 1.3$), which was focused down to a beam spot diameter of 35 μm at the focal plane using a telecentric lens with a focal length of 100 mm and FOV of 40 × 40 mm^2. As it was already stated in Section 2, variations of BIA from normal are always present when processing curved surfaces, which can result in a non-uniform ablation along the beam paths. Therefore, to maintain as consistent as possible ablation along the beam paths regardless of BIA, a quarter waveplate was integrated into the beam delivery system to convert the linear polarisation into a circular polarisation [40]. Moreover, it is worth noting that the four LPTs were initially carried out at a relatively low scanning speed of 10 mm/s in order to characterise the performance of the system under quasi-static conditions. Thereafter, the same tests were repeated at a speed of 100 mm/s to assess the capabilities of the LMM system under dynamic conditions. However, it should be stressed that a constant pulse energy of 50 μJ and a pulse-to-pulse distance of 2 μm was maintained throughout all the experimental procedures, unless otherwise stated.

A fully automated setting up routine, like those in conventional machining, was implemented for correlating the workpiece coordinate system to the machine's one using a CAD/CAM software (GibbsCam). This setting up routine aligns precisely the samples at the focal plane and at the centre of the lens' FOV prior to the LMM operations. In addition, a dedicated module, namely "Laser Process", is integrated into this software which is capable of programming multi-axis LMM movements to execute complex processing strategies. Therefore, it was employed in this research to generate the necessary beam paths and output the respective beam motion commands.

The inspection of the machined structures was performed with the focus variation technology optical microscope (Alicona Infinite Focus G5), which incorporates software tools to perform both surface texture and form measurements on parts with complex 3D geometries. To do so, the system is equipped with a clamping device, which was used for mounting and securing the spherical samples in an exact 90° position and also to move between different machining patterns on them. At the same time, the three integrated linear motorised stages allow X-Y scanning of the processed areas and images of the surface topography to be captured.

Thereafter, each single topography captured was automatically combined into a full 3D model of the machined patterns by using for this the overlapping areas of different scan fields. In the stitching process, any motion errors from the linear stages can be neglected as the system compensates them, automatically. Once the real 3D surface was obtained, a range of software tools were employed to extract the surface forms out of the 3D dataset and then the machined structures were inspected offline.

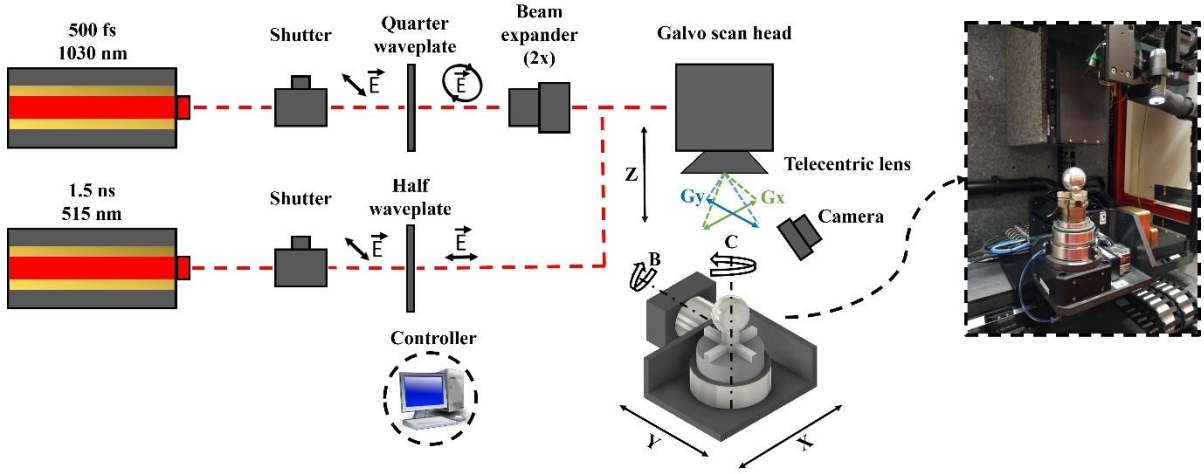

Fig. 6. Schematic illustration of the employed multi-axis LMM set up.

4.2 Process design requirements

Prior to assessing the ARR capabilities of the LMM system, a series of preliminary trials were conducted on planar aluminium substrates. They were used to determine the effective processing window for machining freeform/curved surfaces and also to compensate any negative dynamic effects of the optical beam deflectors. Each experimental procedure was repeated five times to judge the reliability of the obtained results. The machined structures were analysed using the FV microscope with 50x objective lens and lateral and vertical resolutions of 1 μm and 20 nm, respectively.

4.2.1 Effective processing window

To define the effective processing window of the laser source integrated in the LMM system, a vertical scanning strategy was employed to produce scribing lines with a single pass on the surface as depicted in Fig. 7a. Each scribing line was produced with increasing FOD, both above (positive) and below (negative) the focal plane, by moving the Z stage in increments of 100 μm. The laser scribing operations were performed with FODs varying in the range of ± 700 μm, and therefore a relatively large spacing of 200 μm was set between the lines. In this

way, any overlaps between the lines, especially due to the increasing beam spot size, can be avoided. As can be seen in Fig. 7b, significant variations were observed in the ablation depth along the lines processed with FODs in the range from – 700 to + 700 µm. For instance, FOD of ± 300 µm led to an average depth decrease of more than 32%. In this research, the acceptable range of FOD variations, and hence the effective processing window, was defined as a maximum Z offset from the focal plane that entailed an average ablation depth reduction of less than 25% for each scribing line. Therefore, the scribing process was considered effective when the FOD deviations were restricted within ± 200 µm and thus a relatively uniform scribing depth could be maintained along the beam paths. Nevertheless, this is just an assumption in this research and it should be tailored according to the specific laser-material interaction effects that can affect the conducted LPTs.

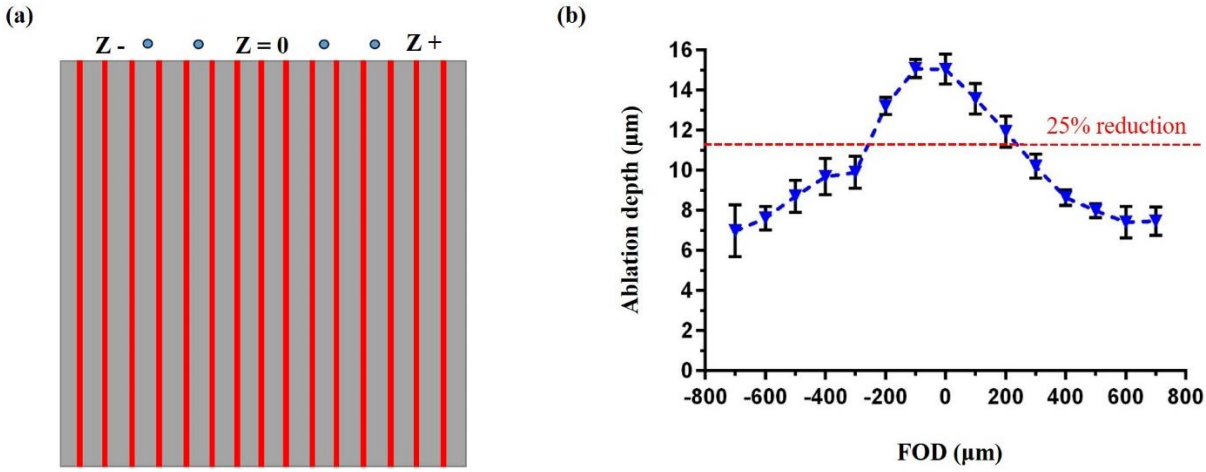

Fig. 7. The effective ablation range analysis: (a) the scribing lines produced with a single pass that were used to identify the acceptable FOD limit; (b) the measured depth of the scribing lines at different FODs.

4.2.2 Dynamic effects of optical beam deflectors

An empirical procedure was implemented to determine the acceleration/deceleration regions of the scan head beam deflectors when used simultaneously with a scanning speed of 100 mm/s. A set of five beam vectors were employed to produce trains of craters on the surface as illustrated in Fig. 8a while the pulse-to-pulse distance was set to 50 µm. Thereafter, the distance between the craters was measured using the automatic fitting tools provided by the 2DImageMeasurement module of Alicona G5 to determine the acceleration/deceleration regions of the beam deflectors. As can be seen in Fig. 8b, a non-uniform distance was observed between the craters at the beginning of the beam vectors owing to their acceleration. Once the

laser beam reached its steady-state velocity, the pulse-to-pulse distance stabilises and as a result the distance between the craters becomes uniform. For example, the average acceleration/deceleration length of the beam deflectors employed in this research was 90.2 ± 0.7 μm at a scanning speed of 100 mm/s. Thus, to ensure a constant velocity along the optical axes during the LPTs, this value was added at the start and end of each beam vector to compensate for the beam deflector's dynamic effects. At the same time, the laser source was switched off during the acceleration /deceleration regions along the beam vectors.

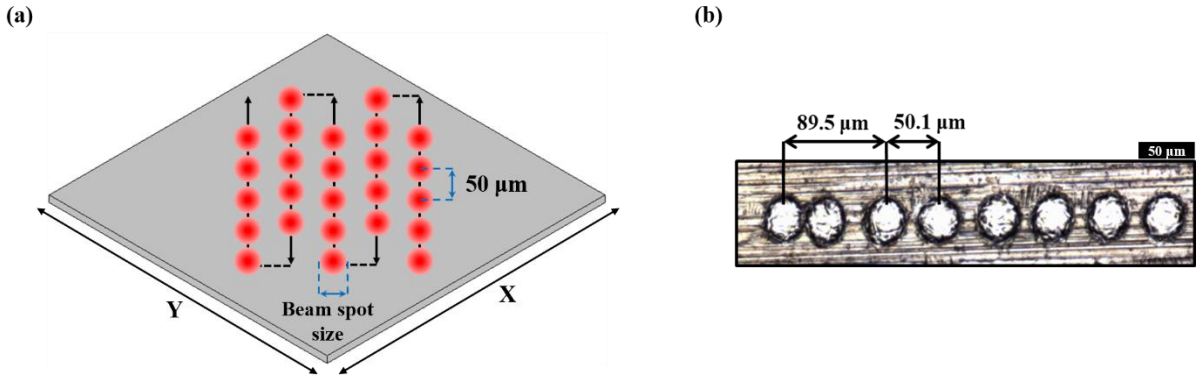

Fig. 8. Analysis of negative dynamic effects along the optical axes: (a) the test procedure used to identify the acceleration/deceleration regions along the beam vectors; (b) the varying craters' distance along one of the beam vectors used to determine the respective acceleration/deceleration regions at a scanning speed of 100 mm/s.

4.3 Design of laser processing tests

The proposed LPTs for assessing the ARR capabilities of the used multi-axis LMM system were implemented as shown in Fig. 9 and the procedure that was followed is explained below in detail. First, an accurate 3D model of the aluminium spheres used in the method pilot implementation was created by using GibbsCAM. Then, the same software was used to design and project the patterns onto the surface of the test sphere. They were four equidistantly 3 × 3 mm^2 square patterns and each of them was used for a different LPT. The size of these four processing fields was chosen so that the FOD variations along the beam paths did not exceed ± 200 μm. A different laser processing strategy was employed to scribe the respective patterns in each test. The desired orientation of the beam vectors in each LPT was defined with guide curves in the used CAD/CAM software that were overlaid onto the 3D sample. Especially, these guide curves determined the direction of mechanical axes' movements during the scribing operations, and thus the beam vectors were oriented perpendicularly to them. It is worth noting that the processing strategies and the combinations of simultaneous multi-axis motions used to

execute each LPT were as defined in Table 1 for a multi-axis LMM configuration with B rotary-axis.

Furthermore, a constant offset distance of 0.2 mm was set between any two consecutive beam scribing vectors and the patterns were produced with a single pass. In addition, three beam vectors, which were 1 mm apart, were also included in the tests to produce reference scribing lines. They would be used to assess the geometrical accuracy, i.e. their *g* to the other scribing lines produced in the LPTs, and also to position the patterns at the centre of the FV microscope's FOV when scribing them. As stated in Sub-section 3.3, the relative positioning movements between these three beam vectors were performed with only the X and Y mechanical axes to achieve the maximum possible accuracy in the used laser processing configuration. At this point, it should be noted that the width of the scribing lines produced on the test pieces was depended on the beam spot diameter at a given FOD and BIA. Based on our initial scribing trials in Sub-section 4.2, variations of scribing lines' width were marginal, within FOD of ± 200 μm. At the same time, taking into consideration both the test piece geometry and the predetermined maximum FOD limit, the BIA variations had a relatively small impact on the resulting scribing lines in the LPTs. Similar observations were also reported in [39], which found that small BIA variations had an almost negligible impact on the morphology of the scribing lines. Thus, the beam spot size and the width of the scribing lines can be deemed constant inside the predetermined effective processing window. Meanwhile, it should be reiterated that the beam vectors were modified as described in the previous section to avoid/minimise the negative dynamic effects of optical axes. Specifically, corrections, i.e. in/out movements for each scribing vector, were introduced in the generated beam paths with GibbsCAM. At the same time, the mechanical axes had a constant velocity that was attained by adjusting the first lead into the beam movement at the beginning of each operation. Finally, a pseudo-repeatability test was performed by repeating the four LPTs on the same sample with a predefined angular displacement of 22.5° from the first patterns along the C axis. Thereafter, a reproducibility test was also carried out on another identical spherical sample using the same laser processing parameters.

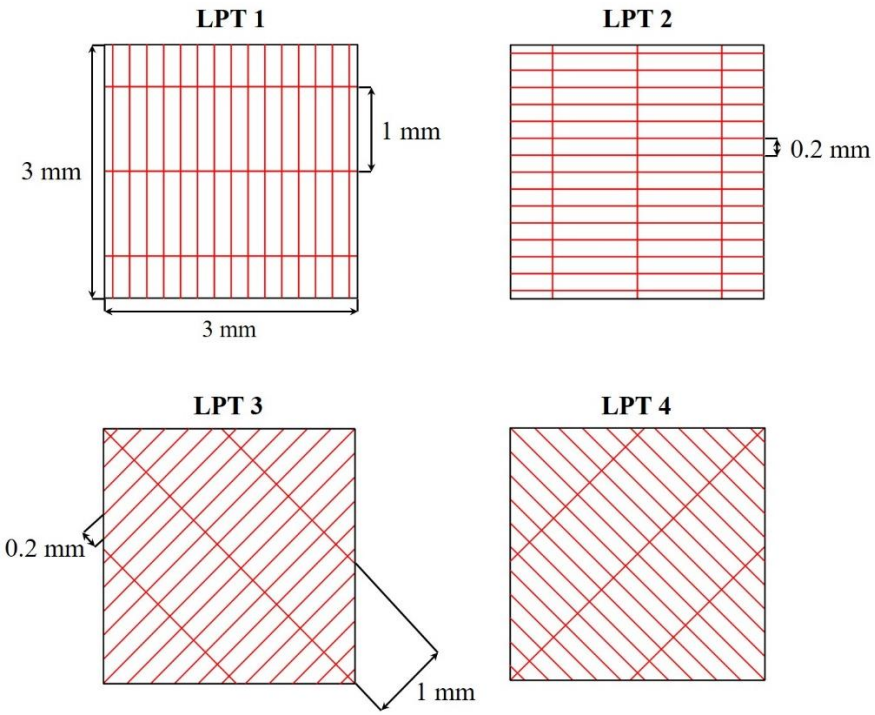

Fig. 9. The implemented LPTs to assess the performance of the employed multi-axis LMM system.

4.4 Uncertainty assessment

The focus variation technology was used for inspecting the scribing lines and quantifying the system's ARR capabilities in this research. Therefore, the uncertainty (u_a) related to the instrument's measurement repeatability was analysed regarding the three measurands. Then, the overall uncertainty (U) in assessing the ARR of simultaneous multi-axis LMM strategies was calculated in accordance to GUM as follows [41]:

$$U_i = max\left(u_{a,i}, u_{b,i}, u_{c,i}\right) \quad (1)$$

where: $i = d_1$, d_2 and g, the measurands used to quantify the processing ARR capabilities; $u_{a,i}$ - the experimental standard deviation of 10 repeated measurements of the same scribing line; $u_{b,i}$ - the experimental standard deviation of repeated measurements on different scribing lines from the two similar patterns produced on the same sample to evaluate the machining repeatability; and $u_{c,i}$ - the experimental standard deviation of repeated measurements on different scribing lines produced on the two samples in order to assess the system's reproducibility. To avoid overestimating the influence of the instrument's repeatability on the overall uncertainty, the largest uncertainty contributor among the calculated type A uncertainties, i.e. (u_a, u_b, u_c), was chosen [42].

Furthermore, the employed measuring procedure itself can significantly affect the instrument's repeatability and consequently the uncertainty in quantifying the system's ARR. Thus, its uncertainty contribution must be minimised in order to perform a reliable analysis. In this regard, a pattern as those produced on the spherical samples in the proposed assessment method was fabricated on a planar substrate and the distance between two lines was measured 10 times as shown in Fig. 10a. It is worth noting that the surface was scanned using only the objectives that provide a lateral resolution better than 1 μm, whilst the measurements were performed by using two methods that minimise the subjective errors associated with the operator. First, the distance between the edges of the 1st and the 2nd lines was measured using the 2DImageMeasurement module available in Alicona software, i.e. by employing an automatic edge detection. Secondly, the distance was measured by using two respective cross-sectional profiles of the lines. Especially, the distance between two points with the maximum depth in these profiles was measured using the ProfileFormMeasurement module. The calculated average values of these measurements and their corresponding standard uncertainties for the considered three Alicona objectives are plotted in Fig. 10b. As expected, the measurement uncertainty decreased with the increase of the objectives' magnification with both measurement methods. A higher scattering of the measurement results was obtained with the second method and therefore the 2DImageMeasurement module was used to perform all the measurements in this research. The measurement uncertainty of this method, employing the three objectives, is stated in Table 3. Considering both the precision of the measurement results and the time required to obtain them, the 50x objective was selected to conduct all measurements in this research.

Table 3. The measurement uncertainty associated with the three objectives when using the 2DImageMeasurement module.

Objectives	Vertical resolution (μm)	Lateral resolution (μm)	u_a (μm)
20x	0.10	0.90	0.9
50x	0.04	0.64	0.5
100x	0.02	0.44	0.3

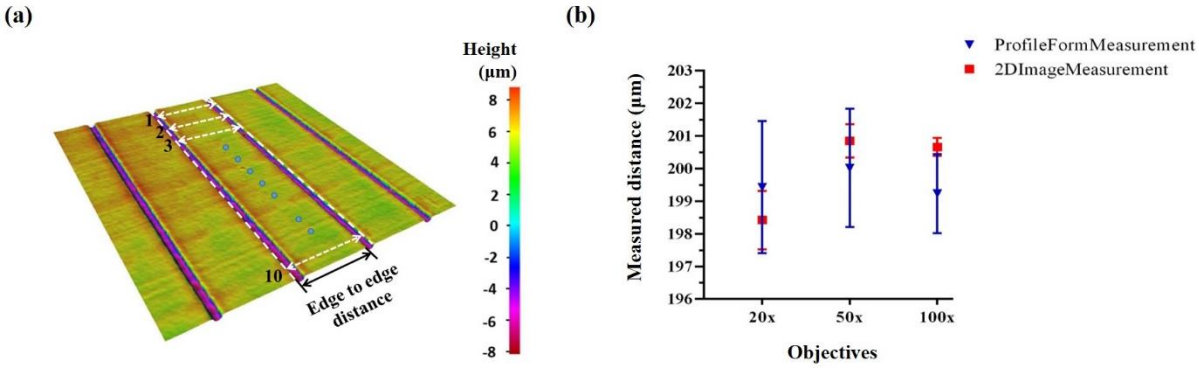

Fig. 10. The measurements conducted by using the two methods: (a) a representative 3D image of the scribing lines with 10 measurements between two consecutive ones; (b) a plot of the standard uncertainties and average values obtained when measuring the distances between two scribing lines with the three objectives and the two methods.

4.5 Results and discussion

The results of the pilot implementation of the proposed methodology are presented and discussed in this section. Fig. 11a-d shows PS 1, i.e. one of the three Pattern Sets produced with the four LPTs on the two samples. 10 different scribing lines on each of the pattern (see Fig. 11a-d) in the three sets, i.e. PS 1, PS 2 and PS 3, were measured to assess the capabilities of the multi-axis LMM system. Especially, the measurements of scribing lines' d_1, d_2 and g were taken on the patterns produced with each test as shown in Fig. 11e. The average value of 10 repeated measurements were used to calculate the deviations from the programmed and executed beam vectors. Since d_2 and g may vary along the scribing lines as stated in Sub-section 3.3, their average values were determined based on repeated measurements taken at 10 and 3 equally distant places along the scribing lines, respectively. By applying the measuring procedure described in Sub-section 4.4, the overall uncertainty, U, associated with the measurands d_1, d_2 and g was better than 0.9 µm, 0.5 µm and 0.1° in this research, respectively.

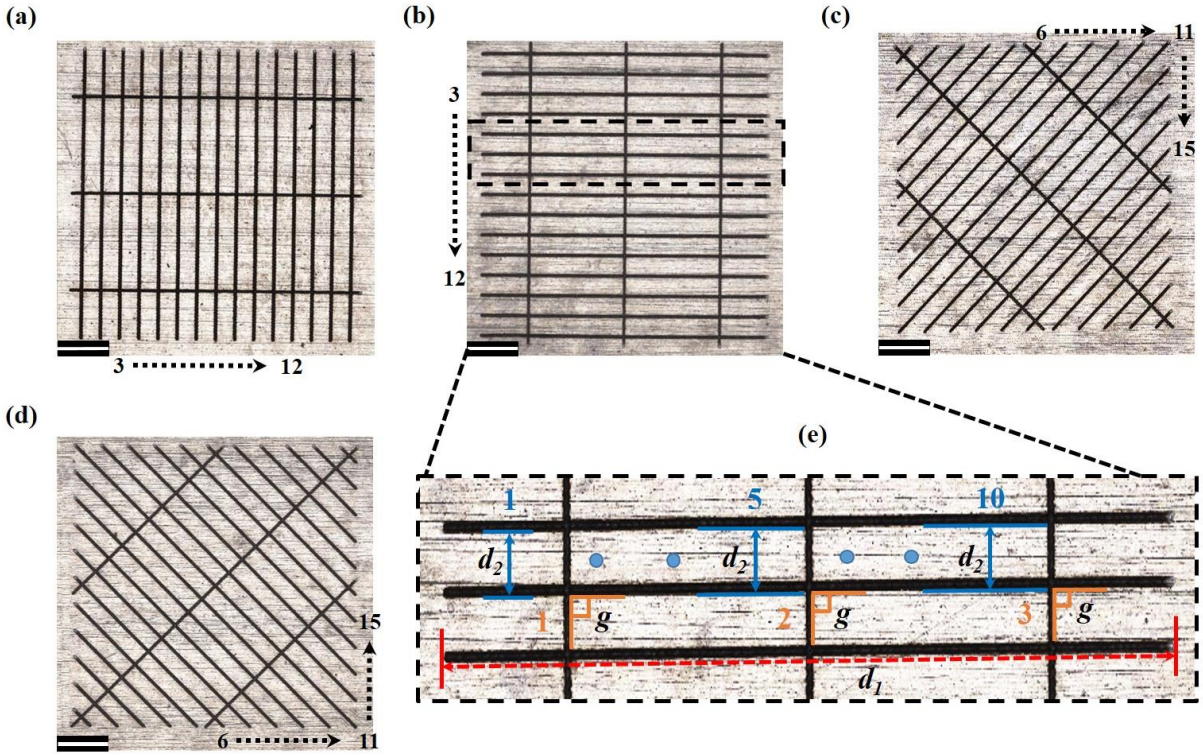

Fig. 11 The patterns in PS 1 that were produced with the four LPTs: (a-d) top view of the four patterns in PS 1 produced with a scanning speed of 10 mm/s; (e) a close view of three scribing lines in (b), which depicts the procedure followed to measure the d_1 (the arrow red dashed line), d_2 (the arrow blue line) and g (the orange 90^0 angle sign).

Note: The black arrow dashed lines and numbers in (a-d) signify the scribing lines measured on the patterns produced in the four LPTs. Scale bar: 500 μm.

4.5.1 Laser processing test 1

The processing ARR achievable when the C rotary-axis is used simultaneously with both optical ones, i.e. the beam deflectors, to execute a given LMM strategy is analysed experimentally in this test. The measurements conducted to assess the system's performance under quasi-static conditions, i.e. when laser processing was carried out at a lower scanning speed of 10 mm/s, are depicted graphically in Fig. 12a-c. The graphs show the deviation of actual measured values from the programmed beam vectors for the scribing lines produced with the vertical scanning strategy in the three Pattern Sets (PSs 1, 2 and 3). As can be seen in Fig. 12a, the maximum deviations observed regarding d_1 of the scribing lines were 32.4 μm, 34.4 μm and 40.5 μm for PSs 1, 2 and 3 on the two samples, respectively. Therefore, it can be stated that the accuracy in executing the beam movements along the programmed beam vectors was better than 40.5 μm. However, the repeatability and reproducibility were less than 3.5 μm

and 7 μm based on the average measurements from samples 1 and 2, respectively. It is evident from these results that the deviations were mainly due to systematic errors and therefore they can be compensated. Conversely, the deviations of d_2 between the scribing lines were much smaller as shown in Fig. 12b. Thus, it can be judged that the accuracy achievable between two consecutive beam vectors was better than 2.9 μm, whilst the repeatability and reproducibility were 1.4 μm and 2.6 μm, respectively. At the same time, Fig. 12c presents the geometrical accuracy of the scribing lines, i.e. their g in regard to the reference ones, in PSs 1, 2 and 3 on the two samples. These results show that the deviation of the scribing lines from their g was less than 0.49°, whereas the respective geometrical repeatability and reproducibility were better than 0.28° and 0.39°, respectively. Finally, the processing uncertainties associated with the conducted LPT were calculated in the same way as the measurement uncertainties using Equation 1. Based on these calculations, it can be stated that the overall processing uncertainty, U, in producing the patterns in LPT 1 was ± 3.7 μm and ± 1.5 μm with regard to the scribing lines' d_1 and d_2, respectively, while regarding their g, it was ± 0.35°.

Thereafter, the same test was performed at a higher scanning speed of 100 mm/s to assess the dynamic performance of the system and the measurement results are presented in Fig. 12d-f. As expected, the dimensional accuracy of the scribing lines worsened as the processing speed increased. More specifically, the accuracy of d_1 and d_2 dropped down to 69.7 μm and 5.4 μm, respectively, while their deviation from g was less than 0.66° based on the results from the three Pattern Sets. Again, the relatively large deviations of the scribing lines' d_1 were mostly due to systematic errors as the repeatability and reproducibility achieved in executing them was found to be 13.3 μm and 17.7 μm, respectively. This was true for their d_2, too, because the repeatability achieved between two consecutive lines was better than 2.5 μm, while the reproducibility was 3.6 μm. On the contrary, it was evident in Fig. 12f that the repeatability and reproducibility in regard to the scribing lines' geometrical accuracy worsened, as the maximum absolute errors obtained when comparing the measured values with the average ones from either one or two samples was 0.62°. Such relatively high geometrical deviations during the machining were mainly ascribed to random errors that would be difficult to compensate/reduce without increasing the overall processing performance of the LMM system. Thus, it can be stated that the processing uncertainty, U, regarding the scribing lines' d_1 and d_2 were ± 10 μm and ± 3.1 μm, respectively, while regarding their g, it was ± 0.63°. Considering the results presented in Fig. 12, it can be concluded that there is an obvious difference between the dimensional accuracy achieved on the sample 1 and sample 2 for both, quasi-static and

dynamic, conditions during this LPT. In contrast, this was not the case regarding the geometrical accuracy (see Figs. 12c and f), as the results obtained from the three Pattern Sets on the two samples were quite similar. This difference can mainly be explained with the use of a reconfigurable work-holding device and/or the precision of mechanical stages employed to position the sample at the centre of the lens's FOV prior to the LMM operations.

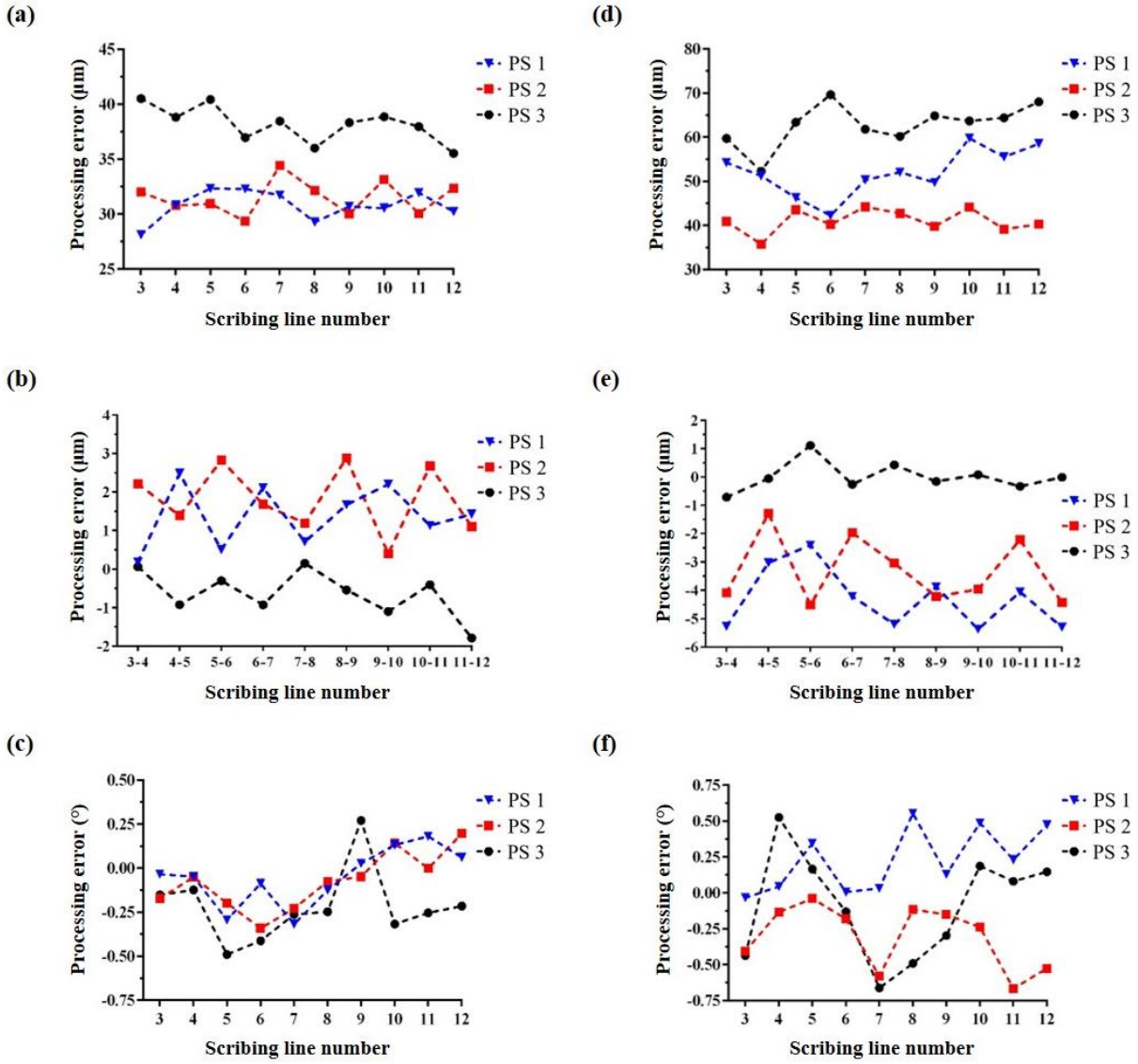

Fig. 12. The effects of multi-axis laser processing errors on d_1, d_2 and g of the scribing lines produced in LPT 1 under quasi-static (a-c) and dynamic (e-f) conditions, respectively.

4.5.2 Laser processing test 2

The aim of this LPT was to assess the processing ARR achievable when 5-axis, i.e. 3 mechanical and 2 optical axes, are utilised simultaneously to execute a given LMM strategy. Initially, the systems' performance was tested at a relatively low scanning speed of 10 mm/s,

especially at quasi-static LMM conditions, and the measurement results are provided in Fig. 13a-c. As can be seen in Fig. 13a, the largest deviation of the scribing lines' d_1 from the programmed beam vectors was less than 40.3 μm based on the measurements of the three Pattern Sets on the two samples. Despite that, the corresponding repeatability and reproducibility achieved was better than 3.4 μm and 6.3 μm based on their average d_1 calculated from the patterns processed on one and two samples, respectively. Once again, the observed deviations from the d_1 of the programmed beam vectors were mostly attributed to systematic errors and hence the processing accuracy can be improved substantially by compensating them. At the same time, it can be noted that there were no significant discrepancies between the LPTs 1 and 2 regarding the scribing lines' d_1. Even though different combinations of mechanical and optical axes were used to execute the beam vectors in these tests, both LMM strategies led to almost equal cumulative errors regarding scribing lines' d_1. Therefore, the dimensional accuracy achieved regarding d_1 might be explained with the cumulative tracking error of the galvo scanner. Nevertheless, this was not the case regarding the d_2 between any two consecutive scribing lines where the errors were higher in comparison to those in LPT 1. Especially, the deviations identified in their d_2 were in the range of 0.4 to 4.9 μm for the three Pattern Sets on the two samples. Thus, the ARR capabilities of the system to execute consecutive beam vectors in producing the three patterns were better than 4.9 μm, 1.6 μm and 2.3 μm, respectively. Moreover, a thorough analysis of the scribing lines' geometrical accuracy revealed that their deviations from g were ranging from 0.1° to 0.5° on the three Pattern Sets. Therefore, the machining ARR achieved regarding the geometry of the three patterns were better than 0.52°, 0.48° and 0.48°, respectively. Finally, it is worth noting that the overall processing uncertainty, U, regarding the scribing lines' d_1, d_2 and g in the LPT 2 was ± 3.7 μm, ± 1.9 μm and ± 0.44°, respectively.

Next, the whole experimental procedure was repeated to assess the influence of dynamic effects on LMM patterns. Figs. 13d-f show the processing errors about the scribing lines' d_1, d_2 and g when the scanning speed was set at 100 mm/s. Generally, the ARR capabilities of the system have worsened significantly under these dynamic conditions. For instance, the dimensional accuracy regarding the scribing lines' d_1, d_2 and g declined to 79.9 μm, 8.7 μm and 0.9°, respectively. At the same time, the negative dynamic effects due to the higher processing speed led to a lower machining repeatability and reproducibility, too. Especially, the repeatability and reproducibility regarding the scribing lines' d_1, d_2 and g under these dynamic conditions were found to be better than 15.3 μm, 4.3 μm and 0.89°, and 28.3 μm, 5.6 μm and 0.85°, respectively.

Thus, it can be stated that the processing uncertainty, U, in regard to their d_1, d_2 and g under these dynamic conditions were ± 15.9 µm, ± 3.1 µm and ± 0.69°, respectively.

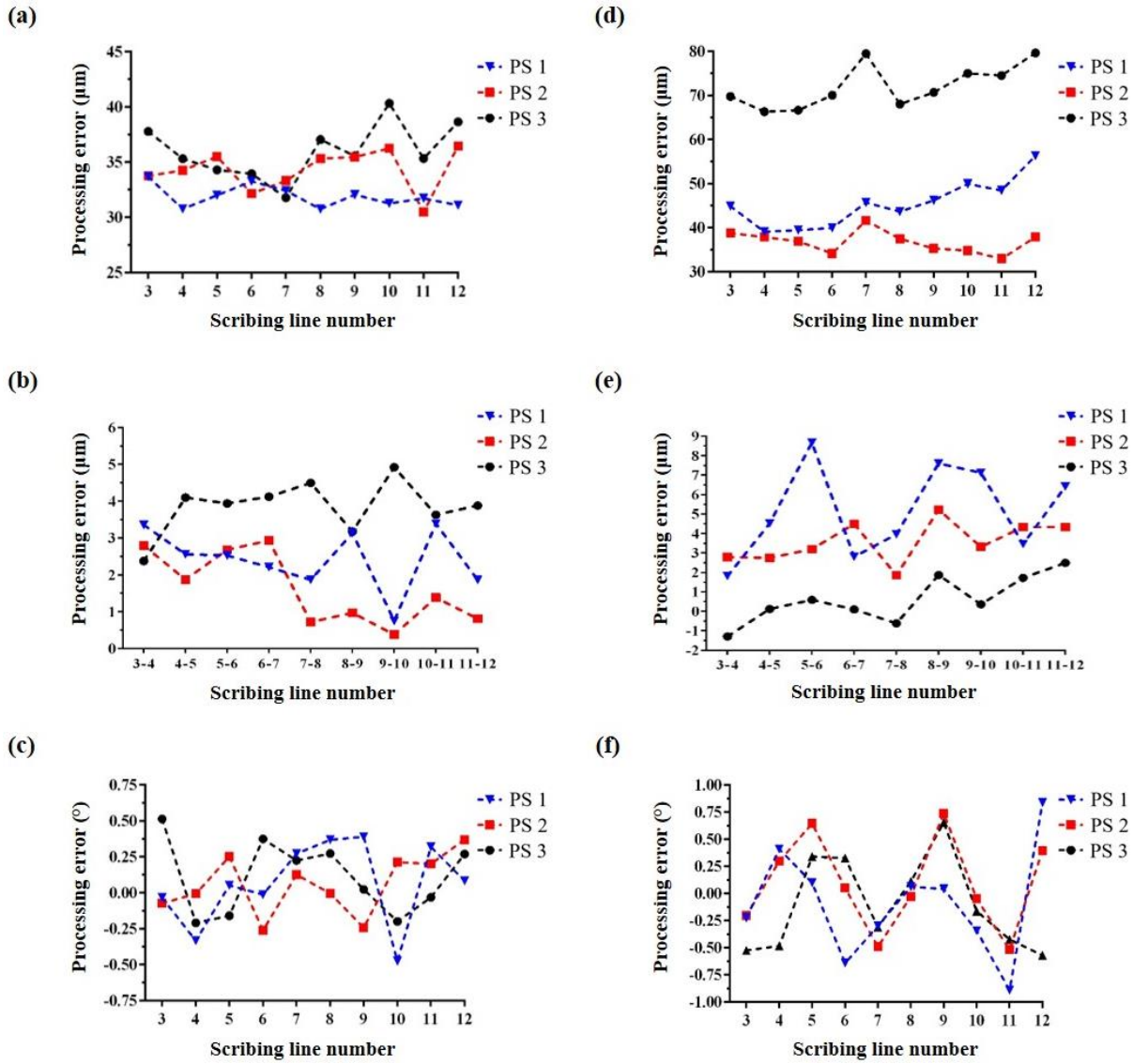

Fig. 13. The effects of multi-axis processing errors on d_1, d_2 and g of the scribing lines produced in LPT 2 under quasi-static (a-c) and dynamic (e-f) conditions, respectively.

4.5.3 Laser processing test 3 and 4

These LPTs aimed to assess the processing ARR achievable when simultaneous 6-axis movements are required to execute a given LMM strategy. Fig. 14 presents the measurement results obtained from the scribing lines processed at a quasi-static conditions, especially at a lower scanning speed of 10 mm/s. Fig. 14a-c displays the deviation of actual measurements from the programmed values for the lines scribed using the diagonal 45° scanning strategy. The analysis of the three Pattern Sets showed that the maximum deviation of d_1 was 62.3 µm.

At the same time, the maximum absolute error with regard to d_2, i.e. the relative distances achieved with two consecutive beam vectors, was 5.0 μm, whilst their deviation from g was 0.52°. On the other hand, the dimensional accuracy of the three patterns produced with the diagonal -45° scanning strategy in LPT 4 was better as it is shown in Fig. 14d-f. It can be seen in Fig. 14d-f that the dimensional accuracy with regard to the scribing lines' d_1 had improved and was better than 45.8 μm. The same applied to the scribing lines' d_2 and g, as the deviations from the programmed values were smaller than those in LPT 3. More specifically, the error regarding d_2 was less than 2.9 μm, whilst their deviation from g was less than 0.38° on the two samples. Therefore, it can be stated that the processing accuracy achieved with regard to the scribing lines' d_1, d_2 and g was better than 62.3 μm, 5.0 μm and 0.52°, respectively, with both 6-axis LMM strategies in LPTs 3 and 4. Additionally, the repeatability achieved in these two LPTs was 19.5 μm, 1.2 μm and 0.48°, and 14.0 μm, 1.4 μm and 0.40° with regard to the dimensional and geometrical accuracy of PS 1 and PS 2, respectively. Thus, it can be stated that the repeatability achieved in the LPTs 3 and 4 was better than 19.5 μm, 1.4 μm and 0.48° about the scribing lines' d_1, d_2 and g, respectively. At the same time, the respective reproducibility achieved in these two tests was better than 19.6 μm, 3.3 μm and 0.48° with regard to the same dimensional and geometrical characteristics of the three Pattern Sets, respectively. Thus, it can be stated that the overall processing uncertainty, U, in producing the three patterns with the simultaneous 6-axis LMM strategies in LPTs 3 and 4 was ± 10.1 μm, ± 1.7 μm and ± 0.42° about the scribing lines' d_1, d_2 and g, respectively.

By comparing the results of LPTs 1 and 2 in Figs. 12 and 13 with those in LPTs 3 and 4, it can be seen that a lower machining ARR was attained regarding the scribing lines' d_1. The relatively lower ARR can be attributed to the varying d_1 of the beam vectors in LPTs 3 and 4. It can be clearly seen in Fig. 14a and d that accuracy gradually decreases with the increase of vectors' d_1 and therefore if the processing errors are normalised, it will be very similar across all vectors' d_1. For instance, after normalising the data obtained from the scribing lines in these two tests, it can be stated that the largest deviation in their d_1 was less than 0.8%.

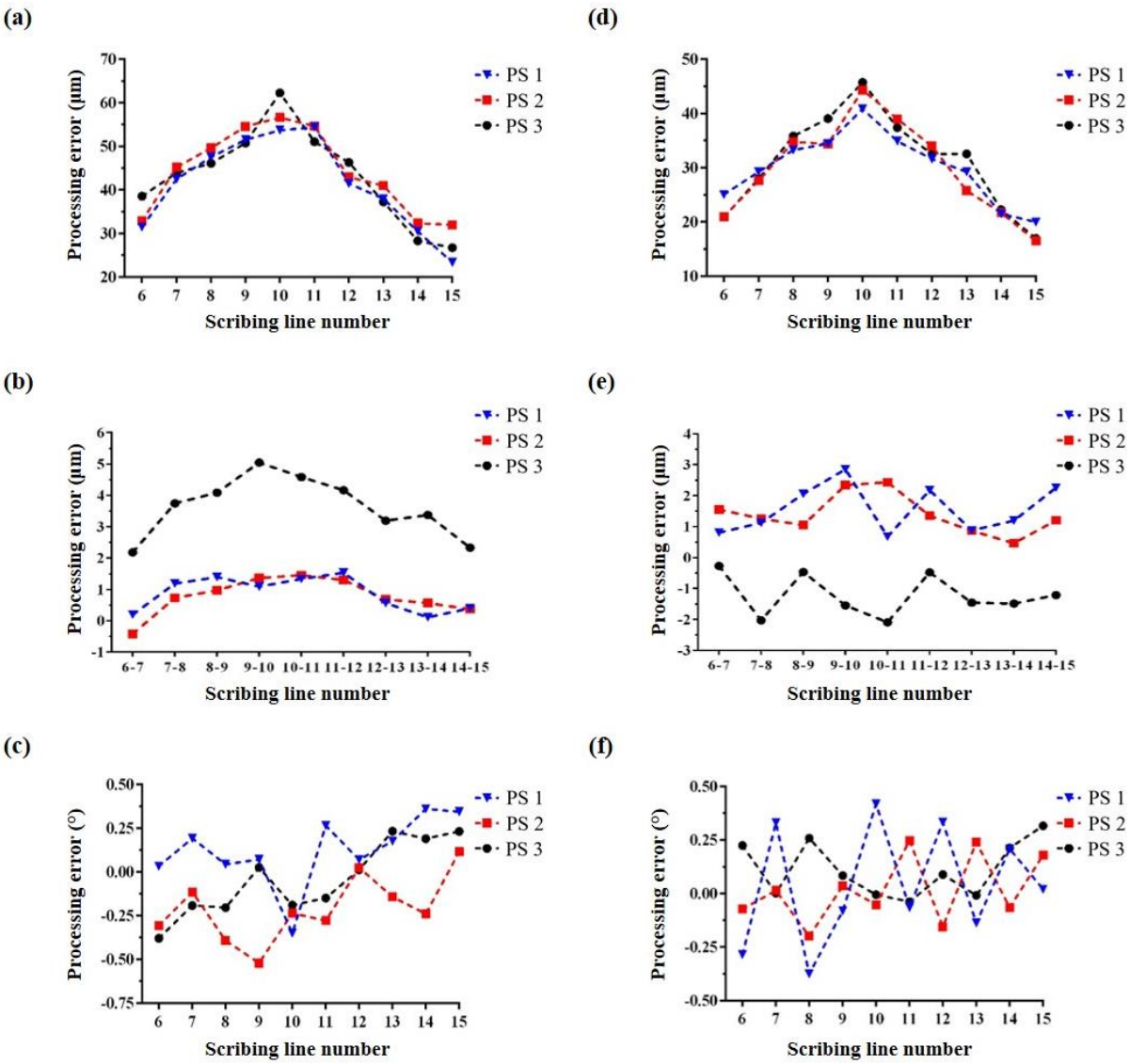

Fig. 14. The effects of multi-axis processing errors on d_1, d_2 and g of the scribing lines produced in LPTs 3 (a-c) and 4 (e-f) under quasi-static conditions, respectively.

The LPTs 3 and 4 were repeated at a higher scanning speed of 100 mm/s to assess, again, the dynamic performance when a simultaneous 6-axis LMM strategy is used, and the results are provided in Fig. 15. Especially, Fig. 15a-c presents the deviations of the actual measured values from the programmed ones when the diagonal 45° LMM strategy was used in LPT 3. As expected, again, the processing errors increased and the dimensional and geometrical accuracies were better than 64.1 μm, 4.9 μm and 0.91° in regard to the scribing lines' d_1, d_2 and g on both samples, respectively. On the contrary, as it was the case with LPT 4 under the quasi-static conditions, the dynamic machining performance was better, again (see Fig. 15d-f). The analysis of the scribing lines of the three Pattern Sets revealed that the processing error regarding the lines' d_1 was less than 58.4 μm, whilst their deviation from g was less than 0.66°.

At the same time, the machining error in regard to d_2, i.e. the relative distances between two consecutive lines, was less than 2.3 μm.

Considering the results obtained in both tests, it can be stated that the processing accuracy was better than 64.1 μm, 4.9 μm and 0.91° in regard to the scribing lines' d_1, d_2 and g, respectively, when the two 6-axis LMM strategies were used. Apart from g, it can be concluded that both LMM strategies achieved a higher accuracy under dynamic conditions compared to the results obtained in LPTs 1 and 2. The superior performance of these 6-axis LMM strategies might partly be attributed to the acceleration/deceleration effects of mechanical axes when executing the programmed beam vectors. For example, the mechanical axes had to adjust their velocity, i.e. accelerate or decelerate, to maintain the scanning speed and compensate for the different distances covered by the optical axes. Additionally, it should be stressed that the effects of multiple geometric errors together with the motion errors of each individual axis were combined and led to the processing errors in both 6-axis LMM tests. As such, some of the factors affecting the machining performance in these two tests might have cancelled each other. Therefore, it can be stated that the proposed method can be used to assess the overall ARR of multi-axis LMM systems but cannot determine the individual contributions of the different axes employed in the tests.

As with the other two tests, the machining repeatability achieved with these two multi-axis LMM strategies was assessed, too. Especially, the repeatability achievable with LPTs 3 and 4 was less than 20.8 μm, 2.2 μm and 0.48° and 17.7 μm, 2.04 μm and 0.81° in regard to the scribing lines' d_1, d_2 and g based on the PSs 1 and 2 results, respectively. Overall, it can be stated that the two simultaneous 6-axis LMM strategies could execute complex beam paths with a repeatability better than 20.8 μm and 2.2 μm regarding the d_1 and d_2 of the scribing lines, respectively, and with a geometrical accuracy better than 0.81°. Additionally, the reproducibility achieved in these two LPTs was 23.2 μm, 2.8 μm and 0.90°, and 18.5 μm, 2.5 μm and 0.86° in regard to the scribing lines' d_1, d_2 and g based on the average results from PSs 1, 2 and 3 on the two samples, respectively. Thus, it can be stated that the two simultaneous 6-axis LMM strategies could execute complex beam paths with a reproducibility better than 23.2 μm and 2.8 μm regarding the d_1 and d_2 of the scribing lines, respectively, while regarding their geometrical accuracy it was better than 0.86°. Overall, the processing uncertainty, U, regarding the d_1 and d_2 of the scribing lines produced with these complex multi-axis LMM strategies was ± 11.1 μm and ± 2.02 μm, respectively, and ± 0.72° regarding their geometrical accuracy.

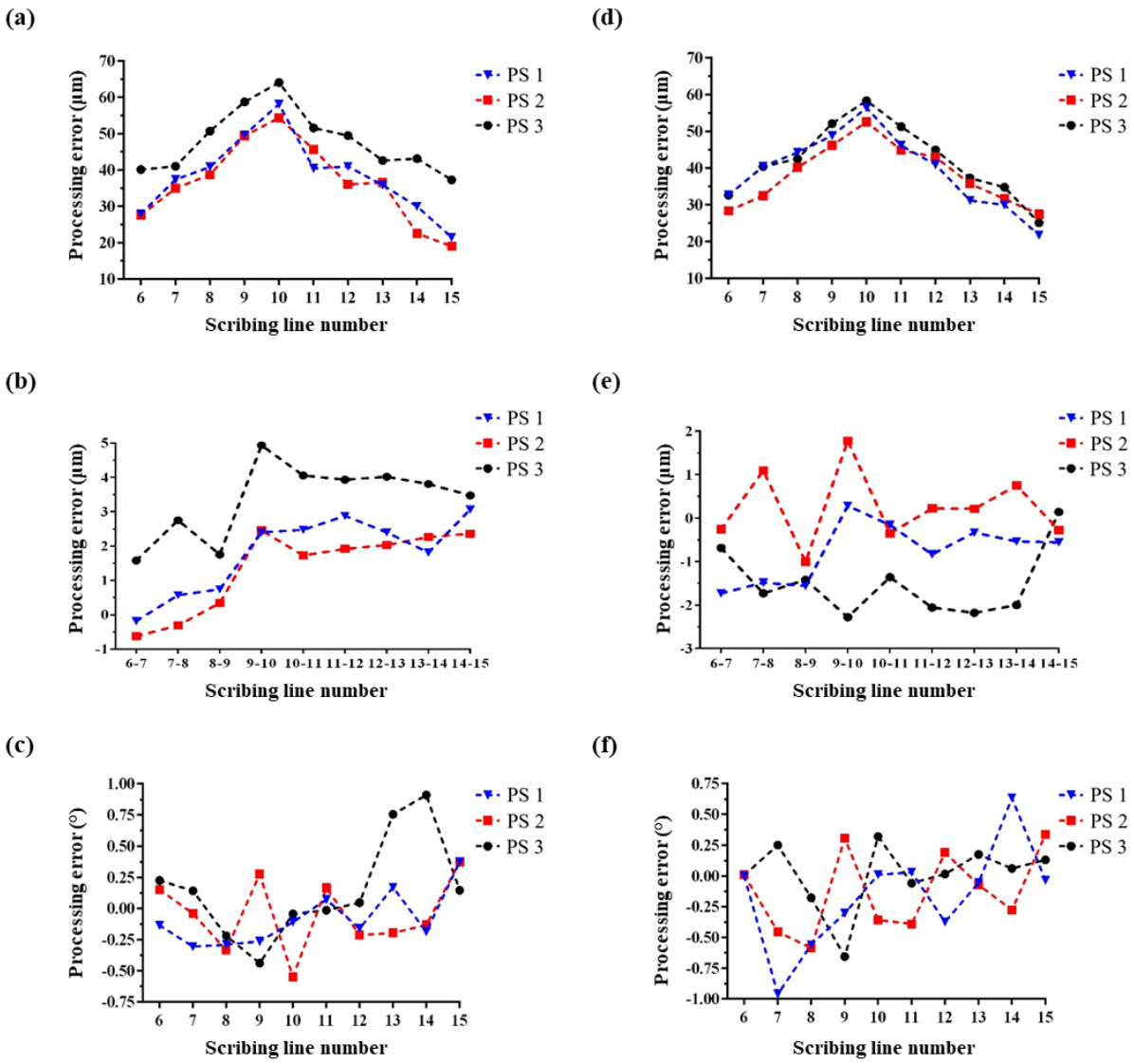

Fig. 15. The effects of multi-axis processing errors on d_1, d_2 and g of the scribing lines produced in LPTs 3 (a-c) and 4 (e-f) under dynamic conditions, respectively.

5. Conclusions

A novel method for assessing the capabilities of multi-axis LMM systems is presented in this paper, especially when executing complex laser processing strategies. The method requires a series of LPTs to be performed on spherical samples when both optical and mechanical axes are used simultaneously. These tests are then employed to investigate and compare the achievable ARR capabilities of such processing strategies under both quasi-static and dynamic conditions. Especially, the tests include strategies requiring the simultaneous use of all possible combinations of optical and mechanical axes available in a given LMM system. By employing this method, the influence of multiple error sources on achievable dimensional and geometrical ARR can be determined when executing any simultaneous multi-axis LMM strategy feasible

on a given LMM system. However, some preliminary trials have to be conducted to implement efficiently the proposed test procedure for a given multi-axis LMM system. Especially, they are important for determining the effective processing window of the integrated laser source, compensating the negative dynamic effects of optical axes and also minimising the measurement uncertainty in quantifying their processing capabilities.

The pilot implementation of the proposed method demonstrates what ARR data could be obtained about any multi-axis LMM strategies when executing processing strategies employing the simultaneous use of up to 6 optical and mechanical axes. In addition, the systematic analysis of the obtained results made possible some generic conclusions to be made about the capabilities of multi-axis LMM systems. Especially, the experimental results revealed that systematic errors were mostly responsible for the relatively low dimensional accuracy in executing multi-axis processing strategies. Therefore, it could be stated in general that the overall system performance of such LMM systems can be improved, substantially, by compensating them. In contrast, it could be stated that the geometrical accuracy achievable with different simultaneous multi-axis LMM strategies could be very similar. However, the respective repeatability and reproducibility achieved could be lower when compared with the dimensional one. In general, the increase of processing speed could lead to an increase of negative dynamic effects on the machining performance of the multi-axis LMM system. When assessing their ARR capabilities, it should be noted that combined processing errors due to the use of different optical and mechanical axes simultaneously are coming into play and they are due to a range of systematic and stochastic factors. Thus, it can be stated that the proposed method can be a valuable tool for assessing the combined effects of multiple geometric errors together with the motion errors of individual axis. Therefore, as such, some of the factors affecting the multi-axis processing performance might cancel each other and these effects could be more pronounced in 6-axis LMM tests. So, it should be stressed that the proposed method can assess, mostly, the overall ARR of multi-axis LMM systems and not the individual contributions of employed optical and mechanical axis. Accordingly, it is reasonable to conclude that this method is more suitable for assessing the overall ARR achievable with such systems. Especially, the proposed methodology can be used after the installation of a given multi-axis LMM system on-site and then after any changes of its multi-axis configuration or after specific time periods to make sure that its overall performance is still within acceptable limits.

Further research should be conducted to evaluate other factors affecting ARR of LMM systems. For instance, the machining accuracy achievable over larger surface areas exceeding the focusing lenses' FOV will be affected by the stitching errors between the processing fields, especially when processing freeform surfaces. Therefore, such stitching errors should be investigated, and ways to minimise them when executing multi-axis LMM strategies have to be proposed. Also, the machining capabilities of LMM systems should be assessed in simultaneous multi-axis strategies that require sharp changes in the motion trajectory of rotary axes and thus to better account for their dynamic performance.

Acknowledgments

The research reported in this paper was supported by a H2020 Factory of the Future projects, "High-Impact Injection Moulding Platform for mass-production of 3D and/or large micro-structured surfaces with Antimicrobial, Self-cleaning, Anti-scratch, Anti-squeak and Aesthetic functionalities" (HIMALAIA) (grant no. 766871). The authors would like to thank the Manufacturing Technology Centre (MTC) for the financial support of Themistoklis Karkantonis's Ph.D. research and acknowledge also the collaboration with LASEA SA, Belgium within the framework of the ESIF project "Smart Factory Hub" (SmartFub) (grant no. 50R18P02795).

References

[1] J. Zettl, M. Klar, S. Rung, C. Esen, and R. Hellmann, "Laser turning with ultrashort laser pulses," *Journal of Manufacturing Processes,* vol. 68, pp. 1562-1568, 2021.

[2] B. Z. Balázs, N. Geier, M. Takács, and J. P. Davim, "A review on micro-milling: recent advances and future trends," *The International Journal of Advanced Manufacturing Technology,* vol. 112, no. 3, pp. 655-684, 2021.

[3] Y. Qin *et al.*, "Micro-manufacturing: research, technology outcomes and development issues," *The International Journal of Advanced Manufacturing Technology,* vol. 47, no. 9, pp. 821-837, 2010.

[4] S. Zhang, Y. Zhou, H. Zhang, Z. Xiong, and S. To, "Advances in ultra-precision machining of micro-structured functional surfaces and their typical applications," *International Journal of Machine Tools and Manufacture,* vol. 142, pp. 16-41, 2019.

[5] P. Penchev *et al.*, "System-level integration tools for laser-based powder bed fusion enabled process chains," *Journal of Manufacturing Systems,* vol. 50, pp. 87-102, 2019.

[6] A. Piqué, R. C. Y. Auyeung, H. Kim, N. A. Charipar, and S. A. Mathews, "Laser 3D micro-manufacturing," *Journal of Physics D: Applied Physics,* vol. 49, no. 22, p. 223001, 2016.

[7] Y. Lin *et al.*, "Durable and robust transparent superhydrophobic glass surfaces fabricated by a femtosecond laser with exceptional water repellency and thermostability," *Journal of Materials Chemistry A,* vol. 6, no. 19, pp. 9049-9056, 2018.

[8] J. G. A. B. Simões, R. Riva, and W. Miyakawa, "High-speed Laser-Induced Periodic Surface Structures (LIPSS) generation on stainless steel surface using a nanosecond pulsed laser," *Surface and Coatings Technology,* vol. 344, pp. 423-432, 2018.

[9] M. Friedrich, M. Seiler, S. Waechter, J. Bliedtner, and J. P. Bergmann, "Precision structuring and functionalization of ceramics with ultra-short laser pulses," *Journal of Laser Applications,* vol. 30, no. 3, p. 032501, 2018.

[10] A. Riveiro, A. L. B. Maçon, J. del Val, R. Comesaña, and J. Pou, "Laser Surface Texturing of Polymers for Biomedical Applications," *Frontiers in Physics,* vol. 6, no. 16, 2018.

[11] Y. Lee *et al.*, "Lubricant-infused directly engraved nano-microstructures for mechanically durable endoscope lens with anti-biofouling and anti-fogging properties," *Scientific Reports,* vol. 10, no. 1, p. 17454, 2020.

[12] G. Xin, C. Wu, W. Liu, Y. Rong, and Y. Huang, "Anti-corrosion superhydrophobic surfaces of Al alloy based on micro-protrusion array structure fabricated by laser direct writing," *Journal of Alloys and Compounds,* vol. 881, p. 160649, 2021.

[13] S. A. Jalil *et al.*, "Creating superhydrophobic and antibacterial surfaces on gold by femtosecond laser pulses," *Applied Surface Science,* vol. 506, p. 144952, 2020.

[14] W. Xing, Z. Li, H. Yang, X. Li, X. Wang, and N. Li, "Anti-icing aluminum alloy surface with multi-level micro-nano textures constructed by picosecond laser," *Materials & Design,* vol. 183, p. 108156, 2019.

[15] T. Chen, W. Wang, T. Tao, A. Pan, and X. Mei, "Broad-Band Ultra-Low-Reflectivity Multiscale Micro–Nano Structures by the Combination of Femtosecond Laser Ablation and In Situ Deposition," *ACS Applied Materials & Interfaces,* vol. 12, no. 43, pp. 49265-49274, 2020.

[16] T. Karkantonis, A. Gaddam, T. L. See, S. S. Joshi, and S. Dimov, "Femtosecond laser-induced sub-micron and multi-scale topographies for durable lubricant impregnated surfaces for food packaging applications," *Surface and Coatings Technology,* vol. 399, p. 126166, 2020.

[17] A. Klos *et al.*, "Ultrafast Laser Processing of Nanostructured Patterns for the Control of Cell Adhesion and Migration on Titanium Alloy," *Nanomaterials,* vol. 10, no. 5, p. 864, 2020.

[18] L. Orazi, R. Pelaccia, O. Mishchenko, B. Reggiani, and M. Pogorielov, "Fast LIPSS based texturing process of dental implants with complex geometries," *CIRP Annals,* vol. 69, no. 1, pp. 233-236, 2020.

[19] K. E. C. Vidyasagar, V. Aggarwal, S. S. Sinha, and S. K. Saha, "Laser based micro texturing of freeform surfaces of implants using a Stewart platform," *Precision Engineering,* vol. 72, pp. 294–303, 2021.

[20] J. Dong, M. Pacella, Y. Liu, and L. Zhao, "Surface engineering and the application of laser-based processes to stents - A review of the latest development," *Bioactive Materials,* vol. 10, pp. 159-184, 2022.

[21] R. Moreddu, V. Nasrollahi, P. Kassanos, S. Dimov, D. Vigolo, and A. K. Yetisen, "Lab-on-a-Contact Lens Platforms Fabricated by Multi-Axis Femtosecond Laser Ablation," *Small,* vol. 17, no. 38, p. 2102008, 2021.

[22] M. Jiang, X. Wang, S. Ke, F. Zhang, and X. Zeng, "Large scale layering laser surface texturing system based on high speed optical scanners and gantry machine tool," *Robotics and Computer-Integrated Manufacturing,* vol. 48, pp. 113-120, 2017.

[23] G. Cuccolini, L. Orazi, and A. Fortunato, "5 Axes computer aided laser milling," *Optics and Lasers in Engineering,* vol. 51, no. 6, pp. 749-760, 2013.

[24] A. Batal, A. Michalek, P. Penchev, A. Kupisiewicz, and S. Dimov, "Laser processing of freeform surfaces: A new approach based on an efficient workpiece partitioning strategy," *International Journal of Machine Tools and Manufacture,* vol. 156, p. 103593, 2020.

[25] X. Wang, J. Duan, M. Jiang, S. Ke, B. Wu, and X. Zeng, "Study of laser precision ablating texture patterns on large-scale freeform surface," *The International Journal of Advanced Manufacturing Technology,* vol. 92, no. 9, pp. 4571-4581, 2017.

[26] A. Michalek *et al.*, "Modelling ultrafast laser structuring/texturing of freeform surfaces," *Applied Surface Science Advances,* vol. 2, p. 100036, 2020.

[27] D. Bhaduri, P. Penchev, S. Dimov, and S. L. Soo, "An investigation of accuracy, repeatability and reproducibility of laser micromachining systems," *Measurement,* vol. 88, pp. 248-261, 2016.

[28] B. Daemi, P. Ekberg, and L. Mattsson, "Lateral performance evaluation of laser micromachining by high precision optical metrology and image analysis," *Precision Engineering*, vol. 50, pp. 8-19, 2017.

[29] P. Penchev, S. Dimov, D. Bhaduri, and S. L. Soo, "Generic integration tools for reconfigurable laser micromachining systems," *Journal of Manufacturing Systems,* vol. 38, pp. 27-45, 2016.

[30] C. Hong, S. Ibaraki, and A. Matsubara, "Influence of position-dependent geometric errors of rotary axes on a machining test of cone frustum by five-axis machine tools," *Precision Engineering,* vol. 35, no. 1, pp. 1-11, 2011.

[31] V. Nasrollahi, P. Penchev, S. Dimov, L. Korner, R. Leach, and K. Kim, "Two-Side Laser Processing Method for Producing High Aspect Ratio Microholes," *Journal of Micro and Nano-Manufacturing,* vol. 5, no. 4, 2017.

[32] S. Ibaraki, S. Tsujimoto, Y. Nagai, Y. Sakai, S. Morimoto, and Y. Miyazaki, "A pyramid-shaped machining test to identify rotary axis error motions on five-axis machine tools: software development and a case study," *The International Journal of Advanced Manufacturing Technology,* vol. 94, no. 1, pp. 227-237, 2018.

[33] Z. Su and L. Wang, "Latest development of a new standard for the testing of five-axis machine tools using an S-shaped test piece," *Proceedings of the Institution of Mechanical Engineers, Part B: Journal of Engineering Manufacture,* vol. 229, no. 7, pp. 1221-1228, 2015.

[34] N. Huang, Y. Jin, X. Li, L. Liang, and S. Wu, "Identification of integrated geometric errors of rotary axis and setup position errors for 5-axis machine tools based on machining test," *The International Journal of Advanced Manufacturing Technology,* vol. 102, no. 5, pp. 1487-1496, 2019.

[35] Z. Zhang, Q. Cheng, B. Qi, and Z. Tao, "A general approach for the machining quality evaluation of S-shaped specimen based on POS-SQP algorithm and Monte Carlo method," *Journal of Manufacturing Systems,* vol. 60, pp. 553-568, 2021.

[36] J. Noh, J. Suh, and S. Na, "Fabrication of Microgrooves on Roll Surfaces Using a Scanner and a Telecentric Lens," *Japanese Journal of Applied Physics,* vol. 49, no. 5, p. 05EC01, 2010.

[37] M. Pothen, K. Winands, and F. Klocke, "Compensation of scanner based inertia for laser structuring processes," *Journal of Laser Applications,* vol. 29, no. 1, p. 012017, 2017.

[38] P. Penchev, S. Dimov, D. Bhaduri, S. L. Soo, and B. Crickboom, "Generic software tool for counteracting the dynamics effects of optical beam delivery systems," *Proceedings of the Institution of Mechanical Engineers, Part B: Journal of Engineering Manufacture,* vol. 231, no. 1, pp. 48-64, 2017.

[39] A. Garcia-Giron, J. M. Romano, A. Batal, A. Michałek, P. Penchev, and S. S. Dimov, "Experimental investigation of processing disturbances in laser surface patterning," *Optics and Lasers in Engineering,* vol. 126, p. 105900, 2020.

[40] L. Overmeyer, J. F. Duesing, O. Suttmann, and U. Stute, "Laser patterning of thin film sensors on 3-D surfaces," *CIRP Annals,* vol. 61, no. 1, pp. 215-218, 2012.

[41] "Uncertainty of Measurement–Part 3: Guide to the Expression of Uncertainty in Measurement (GUM: 1995)," ISO/IEC 98-3:2008, 2008.

[42] G. Tosello, F. Marinello, and H. N. Hansen, "Characterisation and analysis of microchannels and submicrometre surface roughness of injection moulded microfluidic systems using optical metrology," *Plastics, Rubber and Composites,* vol. 41, no. 1, pp. 29-39, 2012.